Design and Development of a Magnetic Anomaly Detection Unmanned Aerial Vehicle

Bruno Miguel Wong Luís
bruno.luis@tecnico.ulisboa.pt

Instituto Superior Técnico, Universidade de Lisboa, Portugal

November 2019

Abstract

This work focuses on the design and development of a new canard fixed-wing vertical take-off and landing (VTOL) unmanned aerial vehicle (UAV) to be used by the Canadian Air Force to conduct Magnetic Anomaly Detection (MAD) operations. An optimized configuration for cruise is obtained for the aircraft. Suitable wing and canard airfoils, shape and dimensions of the lifting surfaces, fuselage, vertical fins, control surfaces are optimized in order to provide the most adequate magnetic interference reduction, functionality, aerodynamics, stability and control characteristics to the aircraft. The definition and implementation of the VTOL architecture is also performed, bearing in mind magnetic interference, power consumption, aerodynamic, structural, vibration and control issues. The best location for the VTOL motors is determined and the transition mode of the aircraft is studied. The designed aircraft, which carries the MAD-XR sensor in its nose in order to reduce the magnetic interference, presents a fine aerodynamic performance at cruise speed, as well as good longitudinal and lateral stability characteristics. The location of the VTOL motors respects the required minimum distances from the MAD-XR sensor, while also meaning a suitable power consumption. The drag due to the presence of the VTOL architecture is estimated. Although the current design fully fulfils the goals established for this work, solutions for possible improvements in future design versions of the aircraft are presented. These solutions are meant to increase aerodynamic efficiency, reduce fuel consumption, increase maximum forward speed and reduce propulsive system mass.

Keywords: Aircraft Preliminary Design, Aerodynamic Optimization, Vertical Take-off and Landing (VTOL), Flight Mode Transition

1. Introduction

1.1. Motivation

This aircraft will look for submarines with the help of a Magnetic Anomaly Detection sensor carried as payload in its nose. The magnetic noise generated by the inboard components of the aircraft cannot exceed tolerable values (defined by the Canadian Air Force) in the MAD sensor.

Most of this aircraft's mission time is spent in cruise, thus a design with optimum aerodynamic, static and dynamic stability characteristics in cruise is of utmost importance.

This aircraft is also VTOL-capable, hence having the advantages of traditional fixed-wing configurations, but also the capability of taking-off and landing in small areas, such as a ship's helipad. An ideal location for the VTOL motors should be defined.

The propulsive system of this aircraft is comprised of 4 electric motors and 1 pusher fuel engine. During VTOL, the aircraft is solely powered by the electric motors, while in cruise, the aircraft is solely powered by the pusher engine. During transition between VTOL and fixed-wing stages, the electric motors and the piston engine operate together. To understand how the aircraft performs the transition, the evolution of forces and powers should be studied.

1.2. Background

An unmanned aerial vehicle (UAV) is the name given to any aircraft that flies without a human pilot onboard during its operations. UAV are used in several civil and military applications. Within the civil applications, one can highlight package delivery, agriculture, mining and aerial shooting. Within the military applications, one can highlight espionage, enemy detection and warfare.

UAV are also increasingly being used to detect enemy ships, namely submarines. The use of drone technology together with magnetic anomaly detection (MAD) sensors, which are devices that measure magnetic flux density, gives support to this type of missions. In figure 1, a list of UAV performing anti-submarine warfare (ASW) operations is presented.

Figure 1: Top left: Brican TD 100; Top right: Height Technologies PD-1 UAV; Bottom left: HAASW UTAS; Bottom right: MQ-8 Fire Scout

Brican TD 100

TD 100 is a high performance, fixed wing unmanned air vehicle developed by Brican Automated Systems of Brampton, Ontario, Canada [1].

The aircraft has been fitted with two Magnetic Anomaly Detection Systems: the Geometrics from the US and the 1.5 kg (MAD-XR) magnetometer manufactured by CAE in Montreal [1].

In the spring of 2015, the Department of National Defence tested the aircraft's utility for coastal defense and detecting submarines [1].

Height Technologies PD-1 UAV

PD-1 UAV is a multipurpose fixed-wing UAV with a wide range of payloads to fit any mission. Developed by the Dutch company Height Technologies, it is a combat-proven solution that has been officially on service in Ukrainian Armed Forces since 2016 and previously tested for 2 years [2].

PD-1 UAV is used in many civil and military tasks. Among civil tasks, one can point aerial shooting and agriculture. Among military tasks, one can point advanced sea motion detection and border control. Furthermore, since PD-1 UAV is a small drone with low radar and magnetic signature and, hard to detect, it is also used to carry sensitive payload, such as a magnetometer [2].

HAASW UTAS

In January 14, 2015, an article [3] revealed that anti-submarine warfare experts at BAE Systems were developing a UAV sensor payload able to look for submerged enemy submarines by detecting small variations in the Earth's magnetic field. The goal of this drone would be to help US Navy P-8A find submarines from high altitudes.

MQ-8 Fire Scout

MQ-8 Fire Scout is an Unmanned Autonomous Helicopter (UAH) developed by Northrop Grumman - USA in 2009 [4].

This UAV is used for several types of payload, according to its mission. It can carry a MAD sensor and be used to detect surface submarines (with limited capability), however its main application is carrying weapons [4].

2. Aircraft Design Methodology

2.1. Aircraft Design Procedure

Designing an aircraft is a cumbersome task and an iterative step-by-step process is followed so as to fully optimize and understand the characteristics of the aircraft. A flowchart with all the design steps followed is shown in figure 2.

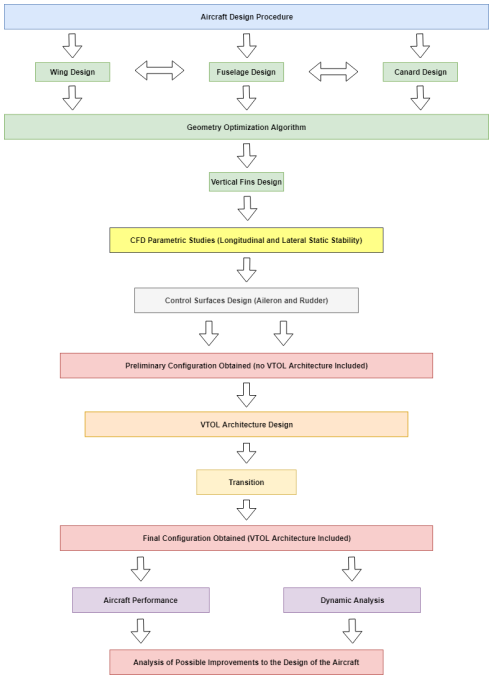

Figure 2: Steps followed during the aircraft design

The design starts with obtaining a first configuration for the aircraft. A wing and a canard are designed to provide a good aerodynamic performance. The fuselage is designed to be able to carry all the internal components, while being aerodynamically efficient as well. The location of the lifting surfaces with respect to the fuselage should provide the aircraft with adequate longitudinal stability characteristics. The desired lateral stability characteristics guide the sizing of the vertical fins.

After obtaining a suitable first design for the aircraft, CFD parametric studies are carried out in order to enhance the geometry of the aircraft.

The control surfaces are sized. Pitch control is achieved with the variation of canard incidence, so the only control surfaces are ailerons and rudders.

Having designed the wing, canard, fuselage, vertical fins and control surfaces, a preliminary aircraft configuration (optimized for cruise, no VTOL architecture included) is thus obtained.

After obtaining this preliminary configuration, important studies regarding the VTOL architecture are conducted. The most adequate location for the VTOL motors is defined based on magnetic interference, power consumption, aerodynamic, structural,

vibration and control requirements.

The aircraft's performance in transition is also studied by looking at the evolution of forces (thrust and lift) and power consumption (VTOL motors and pusher engine) during this stage.

With the VTOL architecture defined and incorporated, a final configuration is obtained for the aircraft. Aerodynamic efficiency, static and dynamic stability analysis of the aircraft are performed. The feasibility and advantages of possible improvements to the current aircraft design are determined.

2.2. Geometry Optimization Problem

To have a first estimate of the most suitable aircraft configuration, a geometry optimization code is developed in MATLAB. The code determines the wing and canard geometries, as well as the location of the lifting surfaces with respect to the fuselage that minimize the ideal power consumption and, achieve a good aerodynamic performance and stability in cruise conditions.

For a certain forward speed V, the optimization statement is as follows:

$$\min_{x} \quad T_p(x) \cdot V \tag{1a}$$

subject to

$$L_w(x) + L_c(x) - W = 0 \tag{1b}$$

$$T_p(x) - D_w(x) - D_c(x) - D_{fus}(x) = 0 \tag{1c}$$

$$M_{acw}(x) + M_{acc}(x) + x_c \cdot L_c(x) - x_w \cdot L_w(x) = 0 \tag{1d}$$

$$9.8 \leq \frac{x_w \cdot a_w \cdot S_w(x) - x_c \cdot a_c \cdot S_c(x)}{\bar{c}_w(x) \cdot (a_w \cdot S_w(x) + a_c \cdot S_c(x))} \cdot 100 \leq 10.2 \tag{1e}$$

$$V_{stall} \leq 20 \tag{1f}$$

$$|\alpha| \leq 10 \tag{1g}$$

$$|\alpha + i_c| \leq 10 \tag{1h}$$

$$0.75 \leq \frac{L_w(x)}{L_w(x) + L_c(x)} \leq 0.8 \tag{1i}$$

$$b_w \leq 4 \tag{1j}$$

x = [α, i_c, b_w, $c_w(y)$, $\theta_w(y)$, b_c, $c_c(y)$, $\theta_c(y)$, x_w, x_c, α_{stall}, i_{cstall}, V_{stall}] is the set of design variables.

The MATLAB code uses the *fmincon* function to find the aircraft geometry, angle of attack α and canard incidence angle i_c that minimize the ideal power consumed by the aircraft for a certain forward velocity (equation 1a). The constraints are the equilibrium equations (equations 1b - 1d), a static margin in cruise around 10% (equation 1e, where only the wing and canard effects are considered), a maximum stall speed of 20 m/s (equation 1f) and, a maximum angle of attack for both the wing and canard limited to 10° (equations 1g and 1h). A ratio of 75% - 80% between wing lift and aircraft lift in cruise is also intended (equation 1i) and, due to space constraints in a ship, the maximum acceptable wingspan is 4 m (equation 1j).

The aerodynamic properties of the wing and canard airfoils are obtained with XFOIL. The code estimates the aerodynamic behaviour of the lifting surfaces through the Lifting Line Theory. The fuselage aerodynamic drag evolution with α is obtained with CFD and used in the code.

The obtention of the most suitable aircraft geometry is an iterative process which not only considers aerodynamic issues, but also magnetic signature, structural, vibration and control constraints.

2.3. Vertical Fins

In [5], the design method to obtain some first dimensions for the vertical fins can be found. In particular, the minimum area of the vertical fins that guarantees enough yaw stability in the aircraft, i.e. $C_{N\beta} \geq 0.001/° = 0.0571/rad$ can be computed.

2.4. CFD Parametric Studies: Longitudinal and Lateral Stability

As for the longitudinal stability, CFD is used to evaluate the possible need to improve the pitch stability. This can be achieved by moving the canard backwards, moving the wing backwards and/or by moving the intended CG forward.

As for the lateral stability, CFD is used to evaluate the possible need to improve the yaw stability. This can be achieved by increasing the area of the fins, increasing the distance between the CG and the aerodynamic center of the fins and/or by adding a third vertical fin. Roll stability is also evaluated with CFD, in particular if wing dihedral is required.

2.5. Control Surfaces Sizing

In [6], the design method to obtain the dimensions of the ailerons and rudders can be found.

2.6. VTOL Architecture Incorporation

When selecting the most suitable location for the VTOL motors, magnetic interference, power consumption, aerodynamic, structural, vibration and control issues are considered.

First of all, it is strictly mandatory to guarantee that all the VTOL motors are placed at a distance of at least 1.35 m from the MAD-XR sensor, as required by the Canadian Air Force.

Minimizing the power consumption during VTOL stages implies smaller, lighter electric motors and batteries, which is beneficial in terms of aircraft weight reduction. Regarding the power calculations, Linear Momentum Theory is used.

The booms that connect the VTOL motors and the structure of the aircraft imply drag penalties.

Minimizing these drag penalties is important to have a more aerodynamically efficient configuration.

The vibration of the electric motors is also a problem. Stiffening the aircraft structure is required.

A minimum thrust-to-weight ratio of 1.5 should be used to guarantee the control and manoeuvrability of the aircraft.

2.7. Transition: Power Studies

According to [7], the aircraft sizing for the transition mode is based on modifying the sizing equations in rotorcraft mode rather than modifying the sizing equations in fixed-wing mode, since it provides more accurate calculations of the required power. The power equations follow from the Linear Momentum Theory and can also be found in [7].

The transition of the aircraft must respect the 3 equilibrium equations (horizontal translation, vertical translation and pitch moment) and the VTOL electric motors should only be switched off once the stall speed of the aircraft is surpassed.

For different forward velocities during transition, it is possible to estimate the aircraft angle of attack α and the canard angle of incidence i_c that guarantee a trim condition, as well as the thrust of the electric motors, the pusher engine thrust, the lift of the aircraft and, the power consumed by the electric motors and by the pusher engine in quasi-static conditions.

2.8. Aircraft Performance Analysis

After obtaining a final configuration for the aircraft, already optimized for cruise and with the VTOL architecture incorporated, a final aerodynamic, static and dynamic stability analysis is performed. As for the dynamic stability analysis, the eigenvalues of the aircraft are computed for different velocities using the equations from [8].

The feasibility and advantages of possible improvements to the current design are presented.

3. Aircraft Design - Implementation and Results

3.1. Wing and Canard Airfoils

The airfoils of the wing and the canard must respect the following conditions:

- Lift-to-drag L/D maximization
- The canard must stall before the wing so as to avoid irrecoverable aircraft pitch-up moment [9].
- Stall proofing requires the canard stall angle to be smaller than the wing stall angle. One way to accomplish so is to have the canard airfoil more cambered than the wing airfoil [9]

The wing has a $\bar{Re} = 8.33333 \times 10^5$ and the canard has a $\bar{Re} = 4.28571 \times 10^5$. Figure 3 provides comparisons between the aerodynamic characteristics of different airfoils from the NACA family.

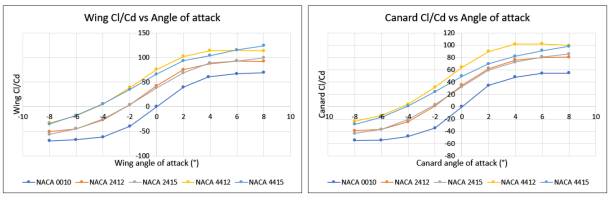

Figure 3: Left image: Wing airfoil comparison at $\bar{Re} = 8.33333 \times 10^5$. Right image: Canard airfoil comparison at $\bar{Re} = 4.28571 \times 10^5$

As for the canard, the airfoil that maximizes L/D for angle of attack values in cruise conditions is the NACA 4412 and it is therefore selected.

As for the wing, due to stall requirements, its airfoil must be less cambered than canard airfoil, so NACA 4412 and 4415 airfoils are ruled out of selection. From the remaining airfoils, NACA 2412 is the one that maximizes L/D for angle of attack values in cruise conditions and it is therefore selected.

3.2. Wing Design

The wing has a span b_w of 3.67 m and a mean chord $\bar{c}_w$ of 0.35 m. The chord distribution generates the wing shape shown in figure 4. As for the twist distribution, the root has a higher angle of incidence than the tip, making the airplane more stable and more resistant to entering a spin. A higher root incidence also assures some aileron effectiveness during stall, giving a greater control of the aircraft.

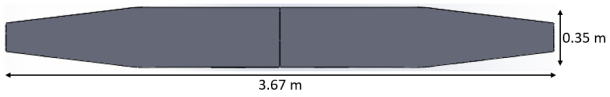

Figure 4: Wing geometry

The aerodynamic characteristics of the wing obtained with the Lifting Line Theory (LLT), Panel Method and Navier-Stokes numerical solution (CFD) are shown in figure 5.

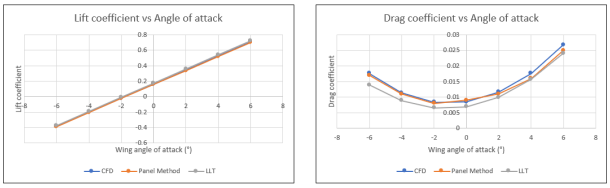

Figure 5: Comparison between results from Lifting Line Theory, Panel Method and CFD analysis

As for the lift coefficient, very similar results are estimated by the 3 theories. As for the drag coefficient, some discrepancies exist between the results estimated by the 3 theories, likely due to the drag models used to assess the friction drag and the boundary layer effect.

3.3. Canard Design

The canard is rectangular and untwisted. It has a span b_c of 1.71 m and a chord c_c of 0.18 m.

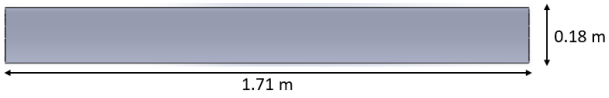

Figure 6: Canard geometry

The aerodynamic characteristics of the canard obtained with the Lifting Line Theory (LLT), Panel Method and Navier-Stokes numerical solution (CFD) are shown in figure 7.

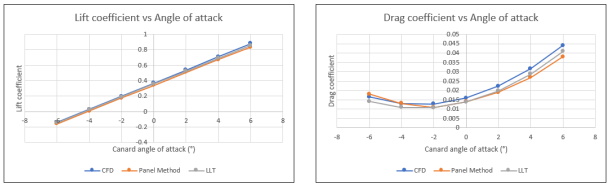

Figure 7: Comparison between results from Lifting Line Theory, Panel Method and CFD analysis

The canard results show similar behaviour as for the wing.

From figures 5 and 7, LLT and CFD estimate close values for the lift properties, however LLT underestimates the total drag of the lifting surfaces.

In the algorithm used for the aircraft preliminary design, the aerodynamic properties of the lifting surfaces are estimated with LLT instead of CFD. Although less accurate, LLT provides analytical equations and avoids the need of developing CAD models and running CFD simulations for different geometries of the lifting surfaces, reducing significantly the workload and time of the process. A more detailed analysis is performed with CFD later.

3.4. Fuselage Design

Figure 8: Longitudinal view of the fuselage with the MAD-XR sensor included

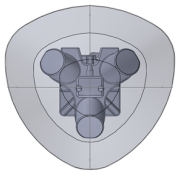

Figure 9: Cross-section view of the fuselage with the MAD-XR sensor included

The fuselage is 3 m long and has a maximum diameter of 0.24 m. A length of 3 m guarantees that the distance between pusher engine and MAD-XR sensor is in accordance with the minimum distance requirements (magnetic interference) defined by the Canadian Air Force.

The drag of the fuselage as function of the angle of attack is plotted in figure 10.

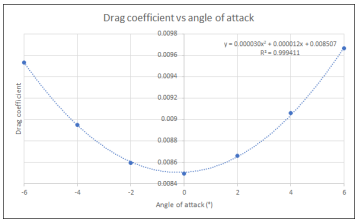

Figure 10: Drag coefficient vs angle of attack

3.5. Vertical Fins Design

A study is conducted to analyse how wing sweep influences the dimensions of the vertical fins to obtain $C_{N\beta} = 0.0571/rad$ and the wing aerodynamics. 3 wing configurations are considered: the wing of figure 4, a wing with 0° leading edge (LE) sweep and a wing with 0° trailing edge (TE) sweep.

From [6], the dimension of the vertical fins necessary to obtain $C_{N\beta} = 0.0571/rad$ for the 3 different wing geometries are compared in table 1.

Wing geometry	**Area** (m^2)	**Height** (m)
0° LE sweep	0.0968	0.6955
Wing of figure 4	0.0794	0.5704
0° TE sweep	0.0673	0.4835

Table 1: Vertical fins dimensions vs wing sweep

The wing with 0° TE sweep yields the smallest values for the size of the fins. With this wing configuration, the distance between the aircraft CG and the aerodynamic center of the fins is bigger, meaning less force to be generated to obtain the same yaw moment. A smaller force means a smaller size for the fins, which is structurally beneficial. Furthermore, having 0° TE sweep does not affect significantly the wing aerodynamic performance. Thus, a wing with 0° TE sweep is used in this aircraft.

3.6. Optimization Algorithm - Configuration Selection

3 possible aircraft configurations were obtained, respectively optimized for the forward speeds of 30 m/s, 35 m/s and 40 m/s.

In table 2, dimensions of the 3 optimized configurations are presented. In figures 11 and 12, plots obtained from the optimization algorithm are presented. The thrust and ideal power required are represented in figure 11. The lift-to-drag ratio of the aircraft is represented in figure 12.

Parameter	30 m/s	35 m/s	40 m/s
b_w	4 m	3.67 m	3.3 m
$\bar{c}_w$	0.37 m	0.35 m	0.34 m
b_c	1.84 m	1.71 m	1.58 m
c_c	0.19 m	0.18 m	0.17 m

Table 2: Wingspan, wing mean chord, canard span and canard chord of the 3 optimized configurations

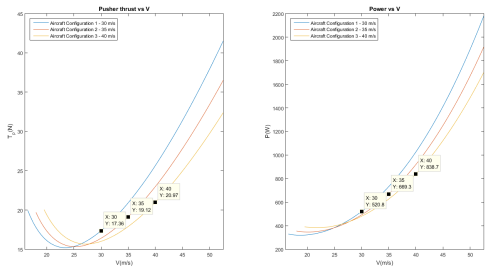

Figure 11: Thrust and ideal power required for the 3 optimized configurations

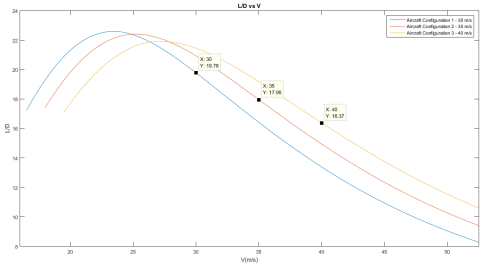

Figure 12: Lift-to-drag ratio of the aircraft for the 3 optimized configurations

Configuration 2 (optimized for a cruise speed of 35 m/s) is selected for the aircraft. Among the 3 configurations, configuration 2 is deemed to present the best balance between aerodynamic efficiency, robustness to wind gusts at sea environment and space constraints. Configuration 2 presents a better aerodynamic performance at the speed it was optimized for when compared to configuration 3, being also more robust to wind gusts and having a smaller wingspan than configuration 1.

The wing, canard, fuselage and vertical fins characteristics can be found in subsections 3.1 - 3.5.

The aircraft has a lift-to-drag of 17.95 and a static margin of 10.01%. The intended CG longitudinal position is 2.095 m. The stall speed is 18 m/s.

3.7. Aircraft Design Improvement using CFD

As for the longitudinal static stability, the preliminary methods yielded a $C_{M\alpha} < 0$ for the aircraft. However, with a more complete CFD analysis, $C_{M\alpha} > 0$, meaning that the aircraft is not actually longitudinally stable. To solve this problem, the wing is moved 9.24 cm backwards and a good static margin is ensured for the aircraft.

As for the lateral static stability, the preliminary methods yielded a $C_{N\beta} > 0.0571/rad$ for the aircraft. However, with a more complete CFD analysis, $C_{N\beta} < 0.0571/rad$, meaning that the aircraft is not actually enough laterally stable. To solve this problem, the height of the fins is increased to 0.6 m and a fin angle of 10° is also used to ensure good yaw stability. No wing dihedral is incorporated, since the roll stability is already quite acceptable.

A high wing/high canard configuration is deemed to be the most appropriate. A high wing is selected, since a MAD mission is better performed with a more stable aircraft configuration. A high canard (with canard and wing at the same level) is selected mainly due to the fact that it is much easier to fit the VTOL architecture and tackle all the structural and vibration issues regarding it. Furthermore, aerodynamic and stability aspects are also found to be acceptable with a high canard.

3.8. Aircraft Configuration (Optimized for Cruise, no VTOL Architecture Included)

The CAD model with the aircraft configuration optimized for cruise, but without VTOL architecture included yet, is shown in figure 13.

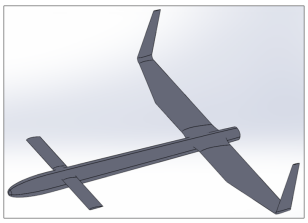

Figure 13: CAD model of the aircraft optimized for cruise, but without VTOL architecture included yet

A better assessment of the aircraft performance is obtained from the CFD results.

The lift-to-drag ratio and trimmed drag polar are represented in figure 14. The thrust and ideal power required are represented in figure 15.

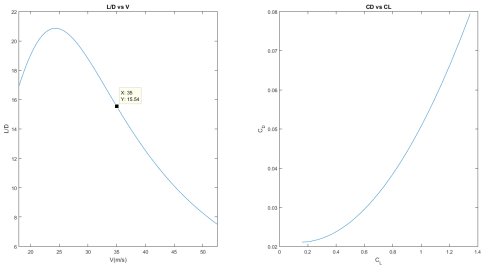

Figure 14: Lift-to-drag ratio for different forward velocities and trimmed drag polar

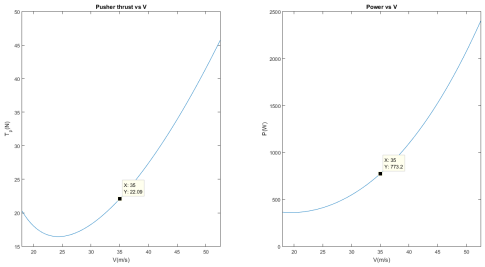

Figure 15: Thrust and ideal power for different forward velocities

The preliminary and CFD approaches yield similar results for the aircraft angle of attack required to guarantee trim condition. As for the lift-to-drag ratio L/D at the cruise speed of 35 m/s, the value estimated with the CFD approach is $\simeq 15.5\%$ smaller than the value estimated with the preliminary approach. The lift coefficient C_L estimated with both approaches is the same, however there is a $\simeq 15.5\%$ increase in the drag coefficient C_D estimated with the CFD approach.

Overall, the aircraft has a lift-to-drag ratio of 15.54 and a static margin of $\simeq 10\%$. The estimated ideal power required at cruise condition is 773.2 W.

3.9. Design of Control Surfaces

Parameter	Value
Inboard position b_{ai}/b_w	0.650
Outboard position b_{ao}/b_w	0.860
Span b_a/b_w	0.210
Chord $c_a/\bar{c}_w$	0.251
Area S_a/S_w	0.053

Table 3: Ratios between the dimensions of the ailerons and the dimensions of the wing

Parameter	Value
Inboard position b_{ri}/b_V	0.100
Outboard position b_{ro}/b_V	0.900
Span b_r/b_V	0.800
Chord c_r/c_V	0.539
Area S_r/S_V	0.431

Table 4: Ratios between the dimensions of the rudders and the dimensions of the vertical fins

3.10. Vertical Take-off and Landing Architecture: Power Calculations

For an axial climb of 2 m/s, total power P is plotted for different positions and radius of the VTOL motors in figure 16. x_F is the distance between aircraft CG and front rotors, x_R is the distance between aircraft CG and rear rotors, R_F is the front rotor radius and R_R is the rear rotor radius.

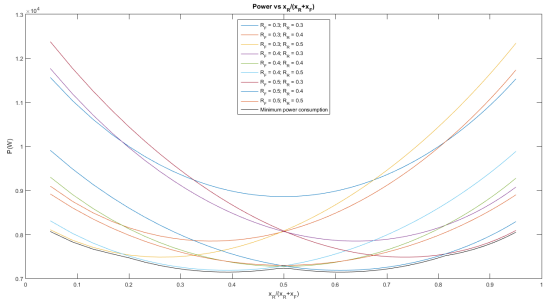

Figure 16: Total power P for different positions and radius of the VTOL motors

The minimum total power consumption occurs when $R_F \simeq 0.4$, $R_R \simeq 0.5$ and $\frac{x_R}{x_R+x_F} = 0.39$ or when $R_F \simeq 0.5$, $R_R \simeq 0.4$ and $\frac{x_R}{x_R+x_F} = 0.61$.

Figure 17 shows the total power increase when the rotors are at a certain position compared to when the rotors are at the positions of minimum theoretical total power consumption.

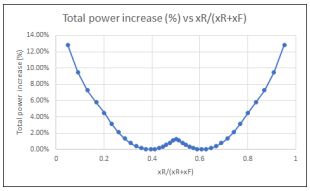

Figure 17: Total power increase for different positions of the front and rear rotors

The differences between having the rotors at the positions of minimum theoretical total power consumption and having the rotors in other positions are limited to a maximum increase of 12.83%. Furthermore, for $0.2 < \frac{x_R}{x_R+x_F} < 0.8$, the power increase is limited to a maximum value of just 4.51%.

3.11. Transition

The evolution of all the forces, as a function of the speed during transition, is provided in figure 18.

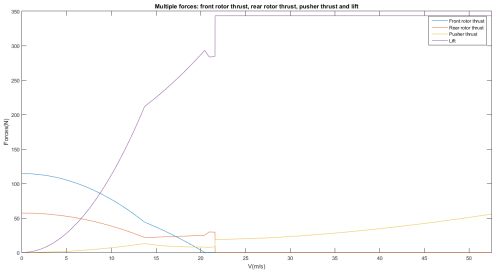

Figure 18: Evolution of forces during the aircraft's transition mode

The evolution of all the powers, as a function of the speed during transition, is provided in figure 19.

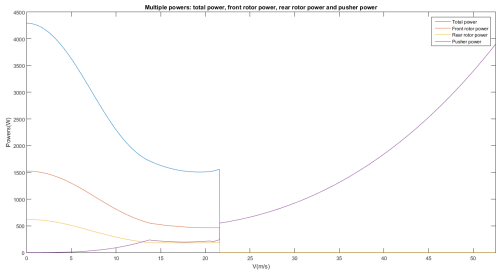

Figure 19: Evolution of powers during the aircraft's transition mode

At very low speeds, the thrust of the VTOL rotors is dominant, since the generated lift is still very small. As the speed during transition increases, the lifting surfaces are capable of generating more lift, meaning that less thrust is gradually required from the VTOL rotors; meanwhile, to propel the aircraft forward, the pusher engine also has more and more influence on the behaviour of the aircraft. For speeds higher than the transition speed, the aircraft is fully powered by the piston engine, namely during its cruise condition.

The sudden change of forces and powers at the transition speed is explained by the fact that when the VTOL rotors are switched off and the thrust contribution is lost, there is a sudden increase in the aircraft lift in order to overcome the weight and trim the aircraft. A sudden increase in the aircraft lift is achieved with a sudden increase in the aircraft angle of attack, meaning also a sudden increase in the aircraft drag, thrust required and pusher power.

4. Aircraft Performance Analysis

4.1. Final Configuration and Aircraft Performance

The CAD model with the final configuration for the aircraft is shown in figure 20.

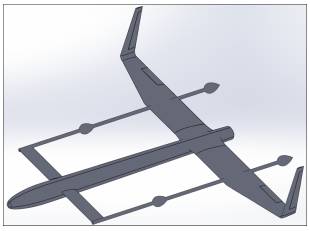

Figure 20: CAD model with the final configuration for the aircraft

The VTOL motors are placed at a distance from the MAD-XR sensor which complies to the requirements regarding magnetic interference.

The VTOL motors are placed in such a way that $\frac{x_R}{x_R+x_F} \simeq 0.67$, which is feasible in terms of control and implies a very small increase in the total power consumption compared to the configurations associated with a minimum total power consumption.

The booms are parallel to the flow, meaning a smaller aircraft drag increase. Stiffening the structure, to counter the electric motors' vibration and respect the aircraft structural integrity, is achieved by connecting the VTOL motors to the rest of the aircraft structure in the way pictured in figure 20.

A final CFD analysis is performed to estimate the aerodynamic properties of the aircraft. The presence of the VTOL architecture is finally considered and, the drag penalties due to its incorporation in the aircraft can be assessed.

The lift-to-drag ratio and trimmed drag polar are represented in figure 21. The thrust and ideal power required are represented in figure 22. The blue lines correspond to the situation in which no VTOL architecture is considered and, the red lines correspond to the situation in which the VTOL architecture is considered. The observed differences are explained by the drag increase due to the presence of the VTOL architecture.

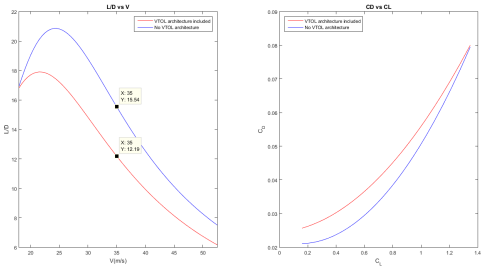

Figure 21: Lift-to-drag ratio for different forward velocities and trimmed drag polar

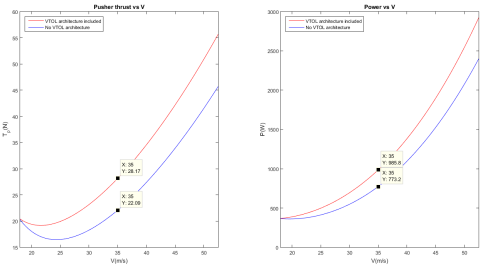

Figure 22: Thrust and ideal power for different forward velocities

The final results for this UAV show a lift-to-drag ratio L/D of 12.19 at the cruise speed of 35 m/s, a stall speed of 18 m/s and an ideal power required at cruise condition of 985.8 W. The incorporation of the VTOL architecture in the UAV implies a L/D reduction of 21.5% and an ideal power required increase of 21.5% (at cruise conditions) compared to when no VTOL architecture was considered.

With the VTOL architecture incorporated in the UAV, the amount of fuel required is 2.45 kg. When

no VTOL architecture is considered, the amount of fuel required is 1.93 kg. The inclusion of the VTOL architecture implies a 26.94% increase in the amount of fuel required to perform the mission.

4.2. Dynamic Analysis

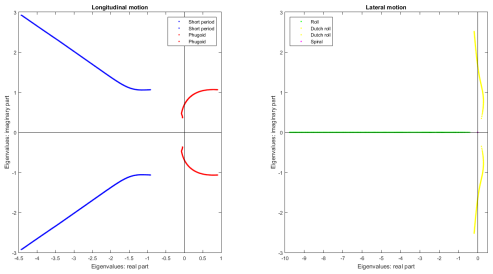

Figure 23: Evolution of the longitudinal and lateral eigenvalues with the forward speed before transition

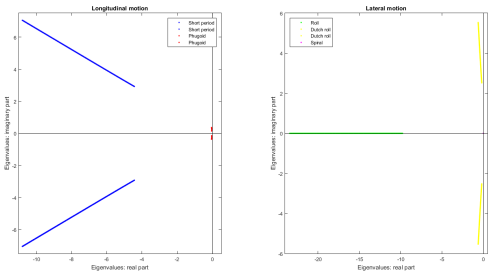

Figure 24: Evolution of the longitudinal and lateral eigenvalues with the forward speed after transition

The evolution of the aircraft eigenvalues with the forward speed before and after transition occurs are plotted in figures 23 and 24, respectively. The longitudinal dynamic modes (short period and phugoid), as well as the lateral dynamic modes (roll, dutch roll and spiral) can be identified.

For speeds below 11.2 m/s, the aircraft is unstable; for speeds above 11.2 m/s, the aircraft is stable.

At cruise speed, the aircraft has the eigenvalues and flying qualities (FQ) shown in table 5.

Dynamic mode	Eigenvalue	FQ
Short period	-7.1973 ± 4.7067 $\cdot i$	Level 1
Phugoid	-0.0374 ± 0.2250 $\cdot i$	Level 1
Roll	-15.6799	Level 1
Dutch roll	-0.3881 ± 3.7924 $\cdot i$	Level 1
Spiral	-0.0094	Level 1

Table 5: Dynamic analysis at cruise speed of 35 m/s

4.3. Possible Improvements to the Design of the Aircraft

Solutions to improve the design for future versions of the aircraft are presented: detachable booms instead of fixed booms for the front VTOL motors and, a tilt rotor instead of the two rear VTOL motors and pusher engine.

Detachable booms for the front motors

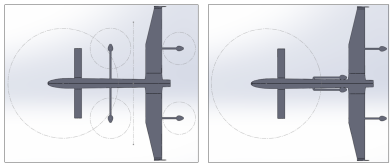

Figure 25: Left image: Configuration in VTOL and transition. Right image: Configuration in cruise

Fixed boom are used in this first/minimum risk design, but detachable booms mean less drag and better aerodynamics in cruise. During VTOL and transition, front motors and detachable booms would be in the position shown in the left image of figure 25. During cruise, the detachable booms would be collected and front motors would be in the position shown in the right image of figure 25.

Use of a tilt rotor

Three advantages arise from this approach: better aerodynamic performance, maximum speed increase and propulsive system mass reduction.

As for the aerodynamic performance, together with the solution of detachable booms for the front VTOL motors, the aircraft in cruise would adopt a configuration quite similar to what is shown in figure 13. UAV aerodynamics is improved and fuel consumption is reduced.

As for the maximum speed of the aircraft, the increase when using a configuration with 1 tilt rotor and when using a configuration with 2 tilt rotors instead of the current configuration is determined for different locations of the rotors. The left and right images of figure 26 show the results when fixed booms and when detachable booms are used to accommodate the front VTOL motors, respectively.

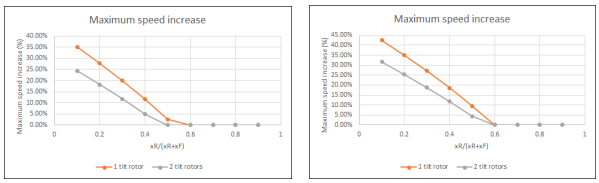

Figure 26: Maximum speed increase

Regardless if the booms are fixed or detachable, when $\frac{x_R}{x_R+x_F} \leq 0.6$, a 1 tilt rotor configuration is preferred to provide the aircraft with a higher maximum speed. For other positions of the rotors, all configurations yield the same maximum speed.

As for the propulsive system mass, the variation when using a configuration with 1 tilt rotor and when using a configuration with 2 tilt rotors instead of the current configuration is determined for different locations of the rotors. A negative variation means a mass reduction, whereas a positive variation means a mass increase.

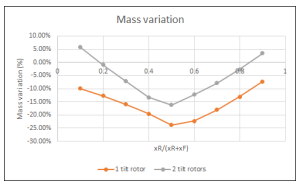

Figure 27: Mass variation

In terms of achieving the highest mass reduction, a 1 tilt rotor configuration should be used regardless of the positions of the rotors. This mass reduction can be used to increase the payload or the fuel amount (range) of the aircraft.

5. Conclusions

5.1. Summary

A new canard fixed-wing VTOL UAV to conduct MAD operations was designed and developed.

First, using preliminary methods and, later, by doing CFD analysis, an optimized configuration for cruise condition was obtained for the aircraft.

After achieving an efficient aircraft configuration for cruise condition, the definition and implementation of the VTOL architecture was performed. The best location for the VTOL motors was determined.

Subsequently, aircraft aerodynamic, stability and power/fuel consumption characteristics were estimated. The aircraft transition mode and dynamic stability behaviour were also analysed.

Lastly, solutions for possible improvements in future design versions of the aircraft were presented.

5.2. Achievements

The designed aircraft presents a good solution and balance between all the magnetic interference, aerodynamic, stability, power and fuel consumption, control, structural and vibration issues.

A fuselage capable of carrying the MAD-XR sensor and other internal components at an adequate distance from the MAD-XR sensor, together with the lifting surfaces, the vertical fins and the control surfaces provide adequate aerodynamic and stability characteristics to the aircraft. A simple and suitable VTOL architecture is implemented, after determining the best location for the VTOL motors and the best strategy to incorporate the booms. Transition is modeled and analysed. The drag and fuel consumption increase due to the presence of the VTOL architecture is estimated.

5.3. Future Work/Recommendations

Future work/recommendations include: ground and flight testing of a proof of concept (to validate the current design of the aircraft and identify issues to be improved in future design versions), use of folding propellers (to reduce drag, noise and vibration of a propeller while not in use), use of magnetic shielding techniques/materials and prevention of magnetic contamination during aircraft manufacturing, assembly and tooling.

Acknowledgements

The author would like to thank his supervisor Professor Afzal Suleman, Dr. José Vale, Dr. Max Rukosuvev, Sean Bazzocchi and the University of Victoria Center for Aerospace Research (UVic CfAR) design team for all the guidance, help and support throughout this thesis.

References

[1] Brican TD100. http://www.navaldrones.com/TD-100M.html. [Online; accessed on March 2019].

[2] Height Technologies PD1 UAV. https://heighttech.nl/wp-content/uploads/2018/10/Techspecs_PD-1.pdf. [Online; accessed on March 2019].

[3] HAASW UTAS. https://www.militaryaerospace.com/articles/2015/01/bae-subhunting-drone.html. [Online; accessed on March 2019].

[4] Fire Scout VTUAV. https://www.naval-technology.com/projects/fire-scout-vtuav/. [Online; accessed on March 2019].

[5] HAW Hamburgh. Empennage Sizing. https://www.fzt.haw-hamburg.de/pers/Scholz/HOOU/AircraftDesign_11_EmpennageSizing.pdf. [Online; accessed on April 2019].

[6] Mohammad Sadraey. *Aircraft Design: A Systems Engineering Approach*. A John Wiley Sons, Ltd., Publication, 2013.

[7] Alex Ramirez-Serrano Ashraf M Kamal. Design methodology for hybrid (vtol + fixed wing) unmanned aerial vehicles. *Aeronautics and Aerospace Open Access Journal*, 2, 2018.

[8] Bernard Etkin and Lloyd Duff Reid. *Dynamics of Flight: Stability and Control*. John Wiley and Sons, 1996.

[9] Snorri Gudmundsson. *General Aviation Aircraft Design: Applied Methods and Procedures*. Elsevier, Inc, 2013.